research papers

A method for the general identification of protein crystals in crystallization experiments using a noncovalent fluorescent dye

**Matthew R. Groves,[a]* Ingrid B.
Müller,[b] Xandra Kreplin[a] and
Jochen Müller-Dieckmann[a]**

[a]EMBL Outstation Hamburg, c/o DESY,
Building 25a, Notkestrasse 85, 22603 Hamburg,
Germany, and [b]Department of Biochemistry,
Bernhard-Nocht-Institüt für Tropenmedizin,
Bernhard-Nocht-Strasse 74, 20359 Hamburg,
Germany

Correspondence e-mail:
groves@embl-hamburg.de

A technique is described whereby the addition of low concentrations (millimolar to micromolar) of the fluorescent dye 1,8-ANS to the protein solution prior to crystallization results in crystallization experiments in which protein crystals are strongly contrasted above background artifacts when exposed to low-intensity UV radiation. As 1,8-ANS does not covalently modify the protein sample, no further handling or purification steps are necessary. The system has been tested on a wide variety of protein samples and it has been shown that the addition of 1,8-ANS has no discernible effect on the crystallization frequencies or crystallization conditions of these proteins. As 1,8-ANS interacts with a wide variety of proteins, this is proposed to be a general solution for the automated classification of protein crystallization images and the detection of protein crystals. The results also demonstrate the expected discrimination between salt and protein crystals, as well as allowing the straightforward identification of small crystals that grow in precipitate or under a protein skin.

1. Introduction

In recent years, great strides have been made towards the production of an integrated X-ray protein crystallography structure-determination pipeline. The processes involved have been broken down into a number of individual steps: automated cloning and purification of proteins (Steen *et al.*, 2006; Hartley, 2006), crystallization (Hiraki *et al.*, 2006), crystal detection in crystallization trials (Berry *et al.*, 2006; Pan *et al.*, 2006; Wilson, 2002), crystal centring (Lavault *et al.*, 2006; Pothineni *et al.*, 2006), data-collection strategies (Bourenkov & Popov, 2006; Popov & Bourenkov, 2003) and structure solution, model building, refinement and validation (Badger, 2003; Kissinger *et al.*, 1999; Panjikar *et al.*, 2005; Mooij *et al.*, 2006; Ness *et al.*, 2004; Perrakis *et al.*, 1997, 2001; Terwilliger, 2004; Terwilliger & Berendzen, 1999). With recent advances, it is now possible to envisage what a fully integrated and automated pipeline would look like.

However, for this pipeline to become a reality, certain conditions need to be met and additional methodologies developed. Primary amongst these new methodologies is the development of a robust protocol for visualizing and identifying crystals that can be applied at multiple stages of the pipeline. Recent publications have suggested a number of methods whereby crystals may be identified and their locations determined. For instance, the programs *XREC* (Pothineni *et al.*, 2006) and *C3D* (Lavault *et al.*, 2006) are a reliable step towards the identification and location of crystals within various cryoloops and may also present a software solution for

the identification of crystals within crystallization images. Other recent publications have suggested the use of native fluorescence (Pohl *et al.*, 2004), UV laser-stimulated fluorescence (Vernede *et al.*, 2006) or modification of the protein sample (Forsythe *et al.*, 2006) as methods to enhance protein crystal identification once mounted upon an X-ray crystallographic beamline

The use of UV laser-stimulated protein fluorescence (266 nm) has been shown to provide significantly increased contrast for the centring of protein crystals such as insulin that contain no native tryptophans to act as fluorophores (Vernede *et al.*, 2006). However, the authors also reported that even short exposures of cryocooled crystals (1 s) to the UV laser resulted in significant radiation damage to a disulfide bond within the protein crystal. While it has been demonstrated that significantly less exposure is necessary for visualization (~20 ms), studies have yet to be performed to determine the effect of millisecond pulses of UV laser light upon the

unprotected crystals present in crystallization trials or upon protein crystallization trials that have yet to produce crystals.

Native protein fluorescence using a low-intensity UV source has also been shown to be of use in the centring of protein crystals on an X-ray crystallographic beamline (Pohl *et al.*, 2004) in a manner similar to that proposed for the use of UV-stimulated fluorescence. However, this application is limited to samples which have significant intrinsic fluorescence. The same intrinsic fluorescence property of proteins has also been suggested to be a means of detecting protein crystals within crystallization experiments (Judge *et al.*, 2005). However, the native fluorescence of proteins is comparatively weak and extremely sensitive to the protein folding state.

A further publication suggests the use of fluorescent dyes to increase the contrast available in crystal visualization, specifically by the covalent modification of proteins prior to the crystallization experiment (Forsythe *et al.*, 2006). While this proposal has the merit of combining the easy visualization
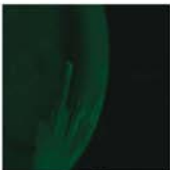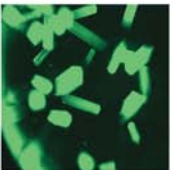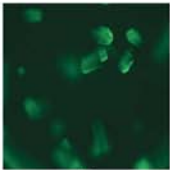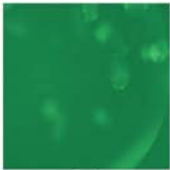

	(a)(i)	(a)(ii)	(b)	(c)
Concentration of 1,8-ANS	9 mM	9 mM	0.9 mM	90 µM
Exposure time (ms)	100	20	100	100
Scale	0–255	0–255	0–255	0–255
	(d)	(e)	(f)	(g)
Concentration of 1,8-ANS	9 µM	0.9 µM	90 nM	9 nM
Exposure time (ms)	100	100	1000 (1 s)	1000 (1 s)
Scale	0–120	0–30	0–30	0–30
	(h)	(i)		(j)
Concentration of 1,8-ANS	0.9 nM	90 pM		H$_2$O control
Exposure time (ms)	10 000 (10 s)	10 000 (10 s)		10 000 (10 s)
Scale	0–30	0–30		0–30

Figure 1
Fluorescence microscopy images collected for lysozyme crystals grown in the presence of decreasing concentrations of 1,8-ANS. In order to display sufficient contrast for visualization, the images were taken with the indicated exposure times and the fluorescence intensities for each image have been artificially colourized, with the indicated scales used (lowest intensities black, highest intensities green). Owing to heavy precipitation at the highest concentrations of 1,8-ANS, (a)(i) is saturated (all pixel values recorded at 255 fluorescence units). Image (a)(ii) is an image taken of the same drop with an exposure time of 20 ms, in which the precipitation and crystal are both visible. The highest concentrations show the strongest fluorescence signals, with decreasing signals obtained as the concentration of 1,8-ANS decreases. Saturation is reached for the highest concentrations and a clear signal above background is still available at a concentration of 0.9 nM. The drop volume is ~4 µl.

through fluorescence imaging in both mounted crystals and in the examination of crystallization trials, it also requires an additional handling step in protein production. The published protocol requires that the target protein is stable in an organic solvent (*e.g.* DMSO), which may limit the general application to a subset of proteins that are stable in this environment. Additionally, further purification steps may also be required to remove any noncovalently bound dye molecules and covalent modification of a protein surface may adversely influence the packing of protein molecules within a crystal lattice.

A further recent publication demonstrated the use of SYBR Green as a tool for the identification of DNA-containing crystals (Kettenberger & Cramer, 2006). The authors reported no adverse effects on DNA–protein complex crystallization and also demonstrated that the large fluorescence signal produced can be used as a means of distinguishing DNA crystals from either salt crystals or from protein crystals which contain no DNA. While this represents a general method for the identification and location of both DNA and DNA–protein complex crystals, it cannot be generally applied to proteins in the absence of DNA.

In this report, we demonstrate that the addition of low amounts of a nonspecific fluorescent dye (1,8-ANS) to a protein sample immediately prior to crystallization results in a significantly enhanced fluorescence signal. 1,8-ANS is a nonspecific fluorescent dye used for protein detection and is also commonly employed in thermal stability assays. In a trial of ten proteins, we show that no significant effect on the crystallization rates from either sparse-matrix screens or from optimization screens can be discerned. The fluorescence signals produced demonstrate a greater contrast in the crystallization images, even allowing direct visualization of small (>1 μm) protein crystals which are formed beneath a protein skin. The greater level of contrast observed also allows clear differentiation of other protein states within the crystallization experiment, such as phase separation and heavy precipitation. Additionally, nonproteinaceous salt crystals produce no significant fluorescence and may thus be discarded as potential leads for further crystallization experiments. Further applications of this method are also briefly discussed.

2. Experimental setup

2.1. Preparation of protein samples

Protein samples were purchased and prepared as follows: lysozyme from Calbiochem, 30 mg ml^{-1} in H$_2$O; insulin from Sigma, 18 mg ml^{-1} in 10 mM Na$_2$HPO$_4$ pH 10; glucose isomerase from Hampton Research, 20 mg ml^{-1} in H$_2$O; xylanase from Hampton Research, 10 mg ml^{-1} in H$_2$O; trypsin from Sigma, 15 mg ml^{-1} in 100 mM Tris–HCl pH 7; proteinase K from Merck, 20 mg ml^{-1} in H$_2$O. In order to assess the suitability of the method using less well characterized samples, a number of protein samples (Rv0153, Rv2234, Ppm1p and Tap42p) were expressed recombinantly and purified to homogeneity following established protocols: Rv0153 (Grundner *et al.*, 2005), Rv2234 (Madhurantakam *et al.*, 2005),

Table 1
Crystallization frequency of lysozyme in the presence and absence of 1,8-ANS in a sparse-matrix crystallization screen.

The conditions in which lysozyme in the absence or presence of 90 μM 1,8-ANS produced crystals in a sparse-matrix screen (Hampton Research Crystal Screens I and II; Jancarik & Kim, 1991), determined by manual inspection, are listed. Conditions which produced crystals in all four trials are highlighted in bold. The experiment was repeated using both commercially available screening solutions and solutions that were prepared manually. Discrepancies between the manual and commercial screen are more likely to be a consequence of nonsystematic errors in the crystallization setup than of genuine errors in the preparation of the reagents.

Concentration of 1,8-ANS (μM)	0		90	
Source of screen	Commercial	In-house	Commercial	In-house
	A7	**A7**	**A7**	**A7**
		A8		
			A9	A9
			B8	B8
	B10	**B10**	**B10**	**B10**
			C1	C1
			C3	C3
	C4	**C4**	**C4**	**C4**
		C7	C7	
	C9	**C9**	**C9**	**C9**
	C10	**C10**	**C10**	**C10**
	D2			
	D3	D3		
	D4			
	E9			
	F3			
		F12		
				G12
	H1		H1	
	H2	H2		
	H3			
	H4			
	H7	H7	H7	
				H10
Totals	15	11	12	11

Ppm1p (Leulliot *et al.*, 2004) and Tap42p (Groves, manuscript in preparation).

2.2. Preparation of the fluorescent dye

The fluorescent dye 1,8-ANS was purchased from Molecular Probes and dissolved to a stock concentration of 90 mM in 10%(v/v) glycerol. The concentration of 1,8-ANS was determined based on an extinction coefficient of 7800 M^{-1} cm^{-1} at an absorbance maximum of 372 nm (emission maximum 480 nm; for further technical details on 1,8-ANS, see http://probes.invitrogen.com/ and Slavik, 1982). Serial dilutions of 1,8-ANS were then prepared in water. Aliquots of the serial dilutions of 1,8-ANS were added to the protein samples prepared as described above at a 1:10 dilution. Once prepared, the serial dye solutions could be stored in a light-proof container at either 277 or 253 K with no significant loss of subsequent fluorescent properties.

2.3. Preparation of crystallization experiments

Once protein samples and dye aliquots had been mixed, as described in §2.2, crystallization trials were performed imme-

diately. Initially, hanging-drop vapour-diffusion experiments were manually set up (McPherson, 1990) in which lysozyme/dye samples were mixed with precipitant solutions (2 µl of each) over 1 ml well solution containing the published crystallization conditions [50 mM sodium acetate pH 4.5 and 5%(w/v) NaCl]. These experiments were repeated three times on each cover slip for each serial dilution of dye that was prepared in order to establish reproducibility. Control experiments in which water was added to the protein samples in a 1:10 ratio were also performed. These experiments were then incubated at 291 K for several days in order to allow crystals to form. Owing to the potential visible light-mediated degradation of 1,8-ANS, these experiments were protected by covering the trays in aluminium foil.

Subsequent experiments were carried out on 96-well plates using the high-throughput crystallization facility at the EMBL Hamburg Outstation. A typical experiment involved the mixing of an aliquot of the dye (or water control) with protein samples immediately prior to automated dispensing of a 300 nl sample against either an equal volume (300 nl) of a previously optimized screen (lysozyme, Ppm1p, Rv2234, Rv0153 and Tap42p) or against commercial or homemade versions of the sparse-matrix screens (Hampton Research Crystal Screen I and II; Jancarik & Kim, 1991; lysozyme, insulin, glucose isomerase, xylanase, trypsin and proteinase K). These experiments were stored in the commercial crystal hotel with no additional protection from visible light for two weeks with no discernible degradation in the function of the dye. Additionally, repeated observation of crystals did not result in any apparent degradation of the fluorescence signal. The formatting of the sparse-matrix crystallization screen is provided as supplementary material[1].

2.4. Visualization of crystallization experiments

The crystallization plates of protein samples tested against the sparse-matrix screen were manually scored for the presence of crystals using images produced from the storage-hotel camera. All subsequent experiments were then visualized under an Axioscope 2 Plus fluorescence microscope (Zeiss, Jena, Germany) either in visible or fluorescence mode. In fluorescence mode, the samples are illuminated by a low-power broad-bandpass UV-light source, with a filter mounted before the objective which removes emission wavelengths lower than 490 nm. Standard procedures were used to protect eyes and skin from exposure to UV radiation. This filter thus removes all fluorescence signals produced by the native protein fluorophores and leaves only the signal resulting from fluorescent transitions of 1,8-ANS. The instrument exposure settings are given where appropriate in §3. All crystallization images presented in this report have been directly output from the fluorescence microscope with no further modification, unless otherwise noted. Image capture was performed using *Openlab* 4.0 (Improvision).

[1] Supplementary material has been deposited in the IUCr electronic archive (Reference: BE5075). Services for accessing this material are described at the back of the journal.

2.5. Diffraction studies on Ppm1p crystals grown in the absence and presence of 1,8-ANS

Crystals of Ppm1p grown in the absence of 1,8-ANS were tested for diffraction properties on beamline BW7B, EMBL Hamburg. Data were collected at 100 K on a MAR345 image plate. Data for Ppm1p grown in the presence of 90 µM 1,8-ANS were collected at beamline X13, EMBL Hamburg at 100 K on a MAR CCD camera. In both cases, data reduction was performed using *MOSFLM* (Leslie, 1992) and refinement was carried out using *REFMAC*5 (Murshudov *et al.*, 1997) using the published coordinates of Ppm1p as a starting model (Leulliot *et al.*, 2004).

3. Results

3.1. Effect of 1,8-ANS on the crystallization behaviour of lysozyme under optimized conditions

In an initial examination of the effectiveness of using 1,8-ANS as a marker for protein crystals, lysozyme was crystallized in the presence of serial dilutions of 1,8-ANS ranging from 9 mM to 90 pM final drop concentration (Fig. 1a–i). For final 1,8-ANS concentrations of less than 9 mM, lysozyme crystals were formed at crystallization rates that were indistinguishable from those in the control, both in terms of overall crystal size and number of crystals present per drop. Examination of the crystallization experiments using visible light indicated that experiments performed in the presence of 9 mM 1,8-ANS (final concentration) resulted in a significantly increased tendency for lysozyme to precipitate (Fig. 1a). This precipitation was not observed under the control conditions, in which 1,8-ANS was entirely absent from the crystallization experiments (Fig. 1j).

Under fluorescence conditions (100 ms exposure), a significant signal was obtained in a 1,8-ANS concentration range of 9 mM to 9 µM (Figs. 1b–e). A further increase of the exposure time (10 s) used to collect the fluorescent images demonstrated that fluorescence associated with the crystals could even be discerned at 1,8-ANS concentrations as low as 0.9 nM (Fig. 1h). Control experiments performed in the absence of 1,8-ANS demonstrate that virtually no native fluorescence signal is present from the lysozyme crystals under these visualization conditions (Fig. 1j). The images collected by the fluorescence microscope are filtered to remove radiation of wavelength <490 nm. As a result, no fluorescence from common protein fluorophores (*i.e.* tyrosine or tryptophan, which have emission maxima at wavelengths in the region of 310–360 nm) is expected and any recorded signal originates from 1,8-ANS.

In order to avoid any precipitation during further crystallization experiments, the remaining experiments were performed using 1,8-ANS concentrations lower than 90 µM (*i.e.* 9 µM and lower). This concentration was arbitrarily chosen as that at which no significant impact on the crystallization or solubility of lysozyme could be observed and under which a strong fluorescence signal could be measured.

3.2. Effect of 1,8-ANS upon the crystallization behaviour of lysozyme in sparse-matrix screens

In the experiment described above, we demonstrated that the addition of low concentrations (micromolar to nanomolar) of 1,8-ANS had no significant effect upon the crystallization of lysozyme under an optimized condition. However, it is also necessary to demonstrate that the addition of 1,8-ANS to sparse-matrix crystallization experiments does not reduce the number of conditions under which lysozyme crystallizes. To this end, we performed a sparse-matrix screening of lysozyme using either a commercially available screen (Hampton Crystal Screens I and II; Jancarik & Kim, 1991) or an identical screen produced by an in-house pipetting robot. Control samples of lysozyme diluted with an aliquot of water were used to establish a baseline number of conditions that resulted in initial crystal hits. Lysozyme samples prepared with serial dilutions of 1,8-ANS were crystallized against the same screens.

The resulting crystallization experiments demonstrated that the addition of 1,8-ANS does not make a significant difference to the crystallization frequency of lysozyme in either the commercial or in-house screens (Table 1). A total of 24 independent conditions were identified in which crystals were grown. On average, lysozyme crystallizes in 13 of these 24 conditions (15 in the commercial screens and 12 in the in-house screens). The addition of 90 μM 1,8-ANS to lysozyme immediately prior to crystallization did not result in a significant change in the rate at which hits were generated from these sparse-matrix screens, with an average of 11 of 24 conditions (11 in the commercial screens and 11 in the in-house screens) yielding crystals (Fig. 2). An examination of the conditions under which crystals were generated demon-strates that cocrystallization of lysozyme with 90 μM 1,8-ANS does not appear to be dependent upon a subset of buffer, precipitant or additive conditions (see Table 1 and supplementary material), with crystals grown over a range of buffer pH values and in the presence of a number of the most commonly used crystallization precipitants in both the presence and absence of 1,8-ANS.

Subsequent fluorescence imaging of the crystallization conditions (Fig. 2) demonstrated that a significantly increased contrast was obtained in the images, with protein crystals clearly visible above all other artifacts in the crystallization experiments (e.g. dust particles, hair fibres, scratches on the crystallization plate etc.). In one condition of the sparse-matrix screen a well formed crystal was grown which did not show significant fluorescence (Fig. 2c). Subsequent X-ray diffraction testing of this crystal indicated that it was a salt crystal, demonstrating the expected utility of this method in distinguishing protein crystals from salt crystals.

3.3. Effect of 1,8-ANS upon the crystallization behaviour of standard proteins in a sparse-matrix screen

In order to demonstrate that the use of fluorescent dyes is of general use in crystal detection, it was necessary to show that fluorescent signals are also produced when 1,8-ANS is mixed with a number of other proteins prior to crystallization. To this end, a number of well crystallizing 'standards' were used: xylanase, glucose isomerase, insulin, proteinase K and trypsin. Insulin represents a useful control for fluorescent imaging as it contains no tryptophan residues and thus has very weak native fluorescence. The samples used for crystallization were prepared as described above in §2.1. No precipitation was
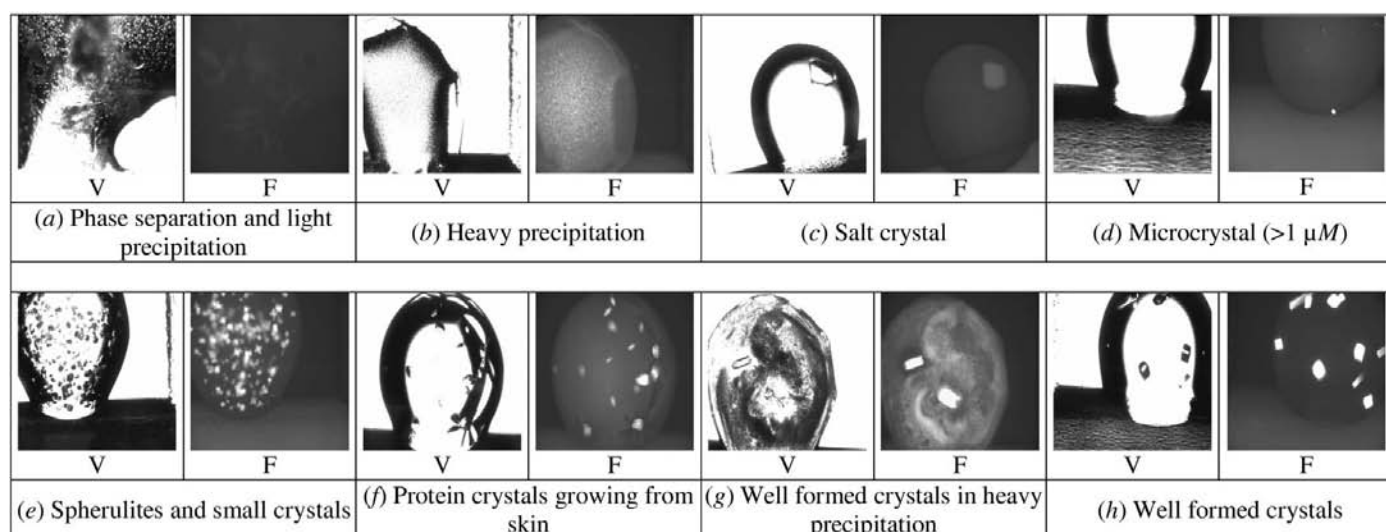
Figure 2
Fluorescence microscopy images of lysozyme crystals grown in the presence of 90 μM 1,8-ANS from a sparse-matrix screen. Visible light (V) and fluorescence (right) images were collected from lysozyme crystallization experiments performed in the presence of 9 μM 1,8-ANS (a–h). Protein crystals grown are contrasted strongly in these images from all other drop features, with even small protein crystals clearly visible (d). Significant differences in the contrast are clearly visible in the cases of phase separation (a), heavy precipitation (b), salt crystals (c), crystals within precipitation (g), spherulites (e) or skin (f) or well ordered crystals (h). All images were taken using an exposure time of 20 ms with no additional processing. The drop volume is ~0.6 μl.

observed upon mixing the proteins with either a 9 µM or 900 nM final concentration of 1,8-ANS.

As can be seen in Table 2, the majority of the control samples crystallized readily in the sparse-matrix screens in the absence of 1,8-ANS. Upon manual scoring of the crystallization images, a total of 100 crystals could be visually identified. The exception is trypsin, which crystallized in only a single condition in the sparse-matrix screens. Further screening around published conditions could potentially increase the number of crystals grown for trypsin and thus expand the scope of our analysis. However, a sample set of 100 crystallization conditions from four independent proteins was felt to be of sufficient size to estimate the effects of 1,8-ANS on the frequency of crystal growth under sparse-matrix conditions. Owing to the high number of samples, no attempt was made to distinguish between salt and protein crystals at this stage.

Crystallization experiments for each of the proteins which produced crystals in the sparse-matrix control described above were performed in the presence of both 9 µM and 900 nM final concentrations of 1,8-ANS, mixed immediately prior to crystallization and the results are summarized in Table 2 (cf. supplementary material). As seen previously for lysozyme, the addition of 1,8-ANS has no discernible effect on the conditions under which these 'standard' proteins crystallize. Of the 100 crystallization conditions determined in which the 'stan-dard' proteins form crystals, the number of conditions that also produce crystals in the presence of 9 µM or 900 nM 1,8-ANS is 72 or 78, respectively. However, potentially as a consequence of nonsystematic errors in the crystallization process, a number of conditions produce crystals in the presence of 1,8-ANS that do not yield crystals in the control samples: the addition of 9 µM or 900 nM 1,8-ANS results in crystals in an additional 27 or 23 conditions, respectively. Thus, the control, 9 µM and 900 nM 1,8-ANS samples produce crystals in a total of 100, 99 and 101 conditions, respectively.

Fig. 3 shows a sample set of the fluorescent images (200 ms exposure) of the protein crystals, in which protein crystals are again strongly contrasted above background levels. It should be noted that all images in this figure are taken under identical conditions and with identical exposure time. The overall levels of fluorescence produced by similarly sized crystals of different proteins demonstrate some degree of variance [e.g. contrast Fig. 3(a) (insulin + 9 µM 1,8-ANS) with Fig. 3(g) (xylanase + 9 µM 1,8-ANS)]. Some degree of variation is to be expected, as 1,8-ANS is environmentally sensitive to the exposed hydrophobic surfaces of proteins and the different proteins used in this study will not have identical hydrophobic surfaces. However, in all cases protein crystals remained the strongest sources of fluorescence within the crystallization experiment and contrasted against any other drop features (e.g. precipitation, phase separation etc.).

	(a) Insulin + 9 µM 1,8-ANS	(b) Insulin + 0.9 µM 1,8-ANS	(c) Glucose isomerase + 9 µM 1,8-ANS	(d) Glucose isomerase + 0.9 µM 1,8-ANS
Exposure time (ms)	100	100	100	100
Scale	0–120	0–120	0–100	0–100
	(e) Proteinase K + 9 µM 1,8-ANS	(f) Proteinase K + 0.9 µM 1,8-ANS	(g) Xylanase + 9 µM 1,8-ANS	(i) Xylanase + 0.9 µM 1,8-ANS
Exposure time (ms)	100	100	100	100
Scale	0–100	0–100	0–120	0–120

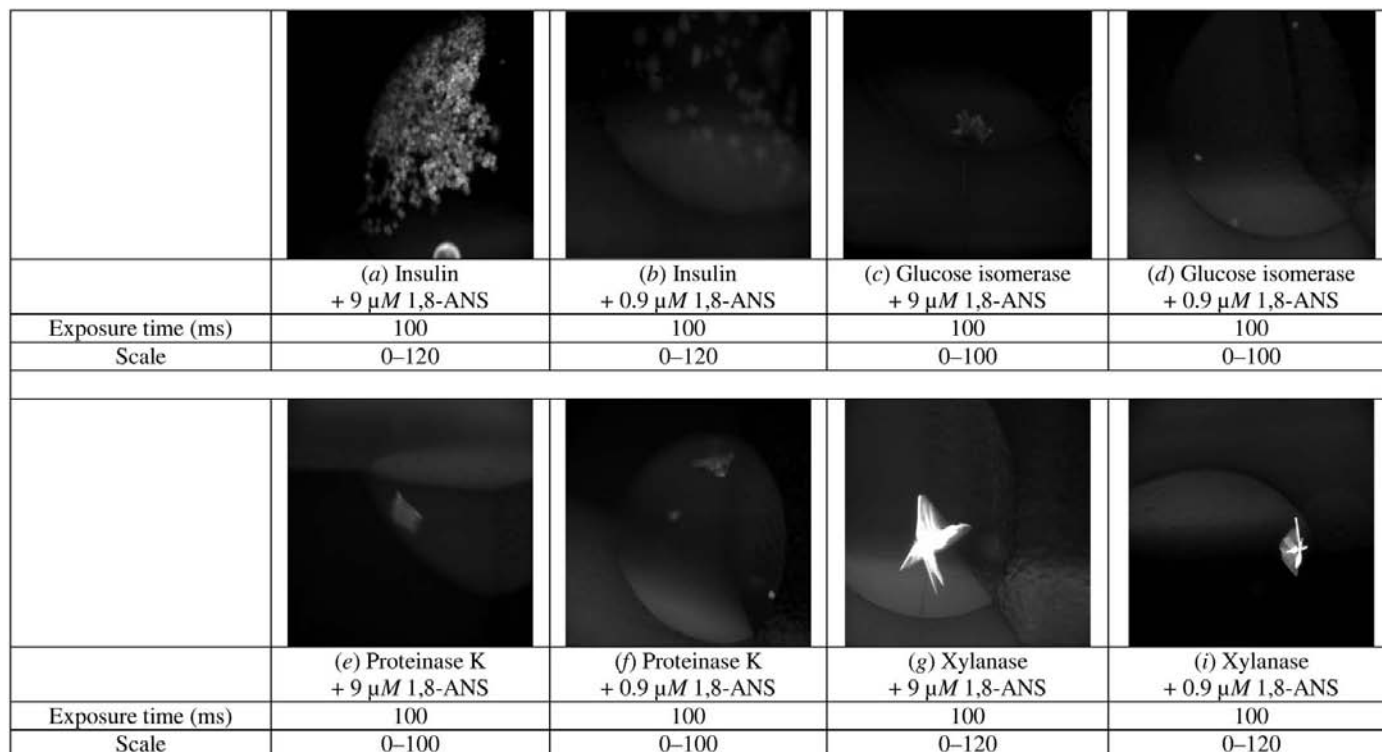**Figure 3**
Fluorescence microscopy images of 'standard' crystals grown in the presence of 1,8-ANS from a sparse-matrix screen. A selection of fluorescence images from proteins crystallized in a sparse-matrix screen in the presence of 9 or 0.9 µM 1,8-ANS are shown. The image exposures and greyscales displayed were adjusted as indicated. The crystals in each condition contrast strongly above the background. Fluorescence signals are stronger for larger crystals and for those grown in higher concentrations of 1,8-ANS. Small crystals (a, d and f) are also visible. Note that crystals grown at lower concentrations of 1,8-ANS (b, d, f and h) display weaker fluorescence signals than those grown at higher concentrations (a, c, e and g). The drop volume is ∼0.6 µl.

Table 2
Crystallization frequency of standard proteins in the presence and absence of 1,8-ANS in a sparse-matrix crystallization screen.

The results of screening a number of protein samples against a sparse-matrix screen (Hampton Research Crystal Screens I and II; Jancarik & Kim, 1991) are shown. Conditions that resulted in crystal growth (as determined by visual inspection of the plates) are indicated by their position on a 96-well plate. Conditions highlighted in bold are those which are unique to the control sample or to samples containing 1,8-ANS. With the exception of trypsin, which produces only a single crystallization condition, the addition of 1,8-ANS makes no discernible change to the crystallization frequency of these proteins in a sparse-matrix screen.

Protein	Final concentration of 1,8-ANS (μM)	Crystallization conditions (96-well plate format)	No. of conditions in which crystals were found
Glucose isomerase	0	A4, A6, **A10**, B2, **B11**, C4, C6, **G1**	8
	9	A6, B2, **B3**, **B5**, **B6**, **B12**, C4, C6, **D3**, **D10**	10
	0.9	A4, A6, **A9**, **B3**, **B6**, **B10**, **B12**, C4, C6, **D10**	10
Xylanase	0	**C8**, C9, **D2**, **F11**, **G8**	5
	9	**B4**, C9	2
	0.9	C9, **H5**, **H6**	3
Insulin	0	**A2**, A6, A8, A9, A10, A12, **B5**, B7, **B10**, C6, C7, C12, **D3**, D4, D5, E11, E12, F5, **F6**, **F11**, G1, G3, G5, G10, H3, H4, H8	27
	9	A6, A8, A9, A12, **B3**, B7, **C2**, **C4**, C6, C7, **C8**, D5, **D10**, E11, E12, **F1**, G1, **G2**, G3, G10, **H2**	21
	0.9	A8, A9, A10, A12, **B3**, B7, **B11**, **C2**, **C4**, C6, **C8**, C12, D4, D5, **D6**, **D8**, **D10**, **E3**, **E6**, E11, E12, F5, G3, G5, **G6**, G10, **H1**, H3, H4, H8, **H10**	31
Trypsin	0	C6	1
	9	—	0
	0.9	—	0
Proteinase K	0	**B2**, B3, B4, B5, B6, B8, B10, B12, C1, C3, C4, C5, C6, C7, C8, C9, C10, C11, C12, D1, D2, D3, D4, D6, D8, D9, D10, D11, D12, E1, E5, E7, E8, E9, F1, F2, F3, F4, F6, F8, F9, F10, F11, F12, G1, G2, G4, G7, G8, G9, G10, G12, **H1**, **H2**, H5, H6, H9, H10, H12	59
	9	**A2**, **A3**, **A4**, **A6**, **A7**, **A8**, **A9**, **A10**, **A11**, B3, B4, B5, B6, **B7**, B8, B10, B12, C1, C3, C4, C5, C6, C7, C8, C9, C10, C11, C12, D1, D2, D3, D4, **D5**, D6, D8, D9, D10, D11, D12, E1, E5, E8, E9, F1, F2, F3, **F5**, F6, F8, F9, F11, F12, G1, G2, G4, G7, G8, G9, G10, G12, H5, H6, **H7**, H9, H10, H12	66
	0.9	**A2**, **A3**, **A4**, **A6**, **A7**, **A8**, **A9**, **A10**, **A11**, B3, B4, B5, B6, **B7**, B8, B10, B12, C1, C3, C4, C5, C6, C7, C8, C9, C10, C11, C12, D1, D2, D3, D4, **D5**, D6, D8, D9, D10, D12, E1, E5, E7, E8, E9, F1, F2, F3, F4, **F5**, F6, F8, F9, F11, F10, F12, G1, G2, G4, G7, G8, G9, G10, H5, H6, H9, H10, H12	67

3.4. Effect of 1,8-ANS upon the crystallization behaviour of 'nonstandard' proteins in optimized screens

While the results achieved in the crystallization of a number of proteins in the presence of 1,8-ANS were encouraging, it could be argued that these samples represent proteins which show a marked tendency to crystallize under a variety of conditions. As such, any inhibitory effects of 1,8-ANS in the crystallization process may be minimized for these samples. A more rigorous testing of the method would be to test the crystallization rates of proteins that have required significant amounts of optimization prior to obtaining high-quality crystals and could be classified as more sensitive to perturbations in crystallization parameters.

Samples of four proteins (Rv0153, Rv2234, Tap42p and Ppm1p) were prepared recombinantly and purified to homogeneity (data not shown). These samples were mixed with 9 or 0.9 μM 1,8-ANS immediately prior to crystallization. In all cases no precipitation was observed upon the addition of 1,8-ANS, indicating that the addition of 1,8-ANS did not adversely affect the solubility or stability of any of these protein samples. Optimization screens were produced centred upon either published conditions (Rv0153, Grundner *et al.*, 2005; Rv2234, Madhurantakam *et al.*, 2005; Ppmlp, Leulliot *et al.*, 2004) or around conditions that had been determined experimentally (Tap42p, Groves, manuscript in preparation). Control crystallization experiments were also performed in the absence of 1,8-ANS.

In all cases crystals were grown from both the control samples and from the samples which contained additional 9 μM 1,8-ANS (Fig. 4 and Table 3). Additional experiments in which a serial dilution series of 1,8-ANS was mixed with protein samples (Table 3) also demonstrate that the overall number of conditions resulting in crystals is approximately constant as the final 1,8-ANS concentration approaches zero (final value 9 p*M*). In the event of an inhibitory effect of the addition of 1,8-ANS, it would be reasonable to expect an increase in crystallization frequency as the final concentration is lowered. Thus, we conclude that the addition of 1,8-ANS plays only a minimal role in the subsequent crystallization rates of the 'nonstandard' proteins in our trial. Additionally, no effect on the overall morphology or size of the crystals grown from the optimized screens could be determined.

3.5. Effect of 1,8-ANS cocrystallization on the diffraction properties of Ppm1p

In order to examine the effects of cocrystallization of proteins with 1,8-ANS, a comparison was made of the diffraction properties of Ppm1p crystals grown in the presence and absence of 9 μM 1,8-ANS. Crystals grown in the presence of 1,8-ANS were illuminated as described above. The crystals produced were of similar size and morphology and, as can be seen from the crystallographic diffraction and refinement parameters (summarized in Table 4), no discernible difference in the diffraction quality could be determined either in terms of resolution limits or from crystal mosaicity. There is no indication in the calculated electron-density maps of the presence of an ordered 1,8-ANS molecule (PDB code 1ob2;

Table 3
Crystallization rates of nonstandard proteins in an optimization screen.

The number of conditions producing crystals in the presence and absence of 1,8-ANS in a screen around the optimal crystallization conditions for each protein are given. The crystallization frequencies are approximately constant across the screen, with no significant increase in frequency as the concentration of 1,8-ANS approaches zero. In each case, the numbers of conditions in which crystals were grown was determined by visual inspection. An example of the fluorescence properties of each crystallization experiment is given in Fig. 3. 'nd' indicates that the experiment was not performed.

Final 1,8-ANS concentration	Rv0153	Ppm1p	Tap42p	Rv2234
No dye (control sample)	1	66	12	23
9 mM	0	65	9	24
0.9 mM	1	55	12	23
90 µM	1	56	13	25
9 µM	1	56	12	24
0.9 µM	3	53	12	23
90 nM	1	56	13	23
9 nM	2	58	12	24
0.9 nM	1	53	nd	nd
90 pM	nd	45	nd	nd
9 pM	nd	49	nd	nd

Table 4
Diffraction and refinement statistics of Ppm1p and Ppm1p in the presence of 90 µM 1,8-ANS.

Data collected on Ppm1p crystals grown in the presence and absence of 1,8-ANS are summarized. No overall change in the diffraction properties can be discerned in terms of the maximum achievable resolution or crystal mosaicity. The changes in unit-cell parameters could potentially be attributed to the presence of 1,8-ANS. Values in parentheses are for the highest resolution bin.

	Ppm1p, no 1,8-ANS	Ppm1p, 90 µM 1,8-ANS
Space group	$P6_5$	$P6_5$
Unit-cell parameters (Å)	$a = b = 110.8$, $c = 166.4$	$a = b = 111.9$, $c = 163.0$
Resolution range (Å)	19.58–1.92 (1.97–1.92)	95.78–1.90 (1.95–1.90)
$I/\sigma(I)$ for highest resolution bin	3.2	4.1
Completeness		99.97
No. of reflections	81264	88060
Mosaicity (°)	0.10	0.08
R_{sym} (%)	3.6	4.1
R factor (%)	20.6 (29.6)	18.2 (23.3)
Free R factor† (%)	26.8 (37.6)	22.4 (30.1)
No. of non-H atoms used in refinement	8633	8781

Protein	**Ppm1p**	**Tap42p**	**Rv0153**	**Rv2234**
Exposure time (ms)	100	100	100	100
Scale	0–200	0–00	0–200	0–200

Figure 4
Fluorescence microscopy images of 'nonstandard' crystals grown in the presence of 1,8-ANS from a sparse-matrix screen. A gallery of crystallization images of the 'nonstandard' protein crystals is shown. All images were taken with a 100 ms exposure in the presence of 0.9 µM 1,8-ANS. The drop volume is ~0.6 µl.

Kouranov *et al.*, 2006). Initial experiments also demonstrated that the fluorescence signal available from the Ppm1p/1,8-ANS crystals is easily detectable when the crystals are mounted on an X-ray synchrotron beamline (data not shown) and further work is also being carried out in this direction.

4. Discussion

It is impossible to guarantee that the addition of 1,8-ANS to crystallization experiments will be suitable for all future applications. Indeed, it is not unreasonable to assume that a number of proteins will not crystallize in the presence of 1,8-ANS. However, in our experiments only a single protein (trypsin) failed to crystallize in conditions containing 1,8-ANS but crystallized in a single condition in the absence of 1,8-ANS. Further screening of trypsin against other standard commercially available screens could yet yield conditions under which trypsin crystallizes in the presence and absence of 1,8-ANS. The 96 conditions tested in our sparse-matrix screens falls someway short of what could be considered to be a full crystal screening, which some researchers have proposed to be of the order of 400–500 conditions (Rupp *et al.*, 2002). Random errors in the crystallization experiments may account for the loss of crystal production, rather than a systematic weakness in the technique in this case.

Although 1,8-ANS interacts nonspecifically with proteins such as lysozyme, the interaction is sufficiently strong at 9 mM 1,8-ANS concentration to result in precipitation of the protein (Fig. 1a). A reduction in 1,8-ANS concentration by a factor of ten (0.9 mM) did not produce any visible precipitation (Fig. 1b). At a final concentration of 9 mM 1,8-ANS, where precipitation of lysozyme was observed, there is an approximately 1:4 protein:dye ratio. However, at 90 µM the protein:ANS ratio is considerably shifted, with the probe as a relatively minor constituent. A potential explanation of the tendency to precipitate is that the addition of 1,8-ANS, which has significant hydrophobic properties, significantly affects the conductivity of the protein solution, which may in turn lead to a stronger tendency for the protein to aggregate. As demonstrated by the structural analysis of Ppm1p grown in the presence of 1,8-ANS, no indication could be found for specific binding of 1,8-ANS to a hydrophobic surface, yet these crystals exhibit strong fluorescence. This indicates that a transient interaction of 1,8-ANS with exposed hydrophobic surfaces or residues, such as those exhibited by the majority of proteins, is sufficient to generate a detectable signal. 1,8-ANS has an absorption maxima at 372 nm, a point at which polypeptides show practically no absorbance (the presence of cofactors may cause an exception to this). Thus, the technique relies on probing the dye environment, rather than the proteins, at wavelengths which do not directly interact with proteins.
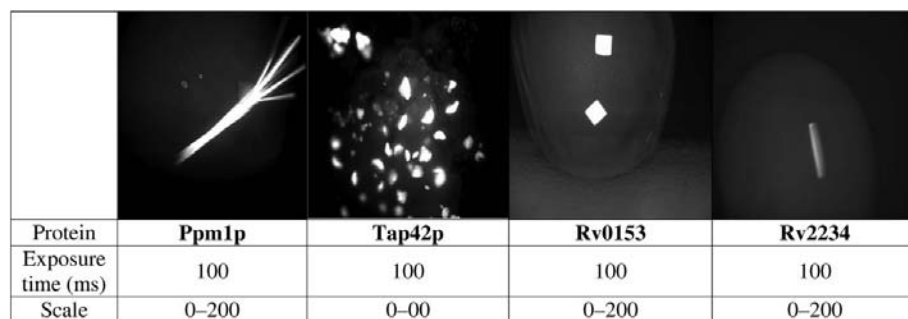
As demonstrated above, the presented technique can easily distinguish between salt and protein crystals, allowing the use of phosphate buffers in crystallization screening. Previously, the use of these buffers has been discouraged owing to the high number of false positives obtained, but it is well known that the use of phosphate buffers may help to stabilize protein solutions at high concentration, as evidenced by the use of such buffers in the majority of NMR experiments.

While the currently available data may not allow robust statistical analysis, an initial estimate for the success rate of ∼90% of protein samples clearly demonstrates that this technique is suitable for inclusion in high-throughput applications. Indeed, the loss of ∼10% of potential crystallization conditions is counterbalanced by the potential for a more robust system for automated crystal detection, which would correctly identify a higher percentage of crystals than the approximately 70–80% quoted by some authors (Berry *et al.*, 2006; Wilson, 2002). As can be seen from Fig. 2, even small protein microcrystals are clearly visible using this technique and such crystals may be difficult to visualize under standard illumination conditions. The potential in adding 1,8-ANS to the crystallization experiment after a given period of time and immediately prior to visualization in order to avoid perturbation of crystal growth has yet to be explored. Certainly, given the rise in use of crystallization robotics and the ability to screen a large number of conditions with limited sample use, it is possible to envisage a crystal-screening process which would include the use of 1,8-ANS in parallel with standard screening without 1,8-ANS. Such parallelization would merely require additional crystallization experiments to be performed.

The benefits of including 1,8-ANS in crystallization trials is highlighted in Fig. 5, in which a cutoff level of 120 (out of 255) fluorescence intensity units has been set for each image. The resulting series of images clearly demonstrates that even small protein microcrystals (Fig. 5*d*) are detectable, whereas drops which contain phase separation, light precipitate or salt crystals (Figs. 5*a* and 5*c*) contain no signal. Thus, an initial segregation of crystallization images is possible through the application of a cutoff level to the fluorescent images. Drops which contain heavy precipitation (Fig. 5*b*) still retain some signal at this cutoff level. However, the fluorescence images contain a greatly increased contrast and a comparison of the efficacy of the crystal-recognition software *XREC* (Pothineni *et al.*, 2006) on a trial sample of visible and fluorescence images demonstrated that the correct identification of drops containing crystals was increased by at least a factor of 50–70%. Future experiments are planned in order to further improve automated recognition of proteins crystals grown in the presence of 1,8-ANS.

The comparison of the structures of Ppm1p solved in the absence and presence of 1,8-ANS indicates that little or no visible damage occurs to the proteins within the crystals upon exposure to the low-intensity UV light used in our experiments. However, the use of 1,8-ANS could be restricted to the identification of crystallization conditions within an initial screening and then subsequently omitted from crystallization optimization trials.

The use of 1,8-ANS was made based upon the particular properties of this dye, which is one of the oldest commercially available dyes, specifically that it has been used to demonstrate the presence of a wide variety of proteins. The modern trend in fluorescence microscopy has been to produce dyes that are more specific, but such products would potentially limit the efficacy of this technique, in which the nonspecificity of the dye is highly advantageous. The use of more modern dyes may indeed provide additional benefits, but with an increase in cost and handling. We are currently testing the
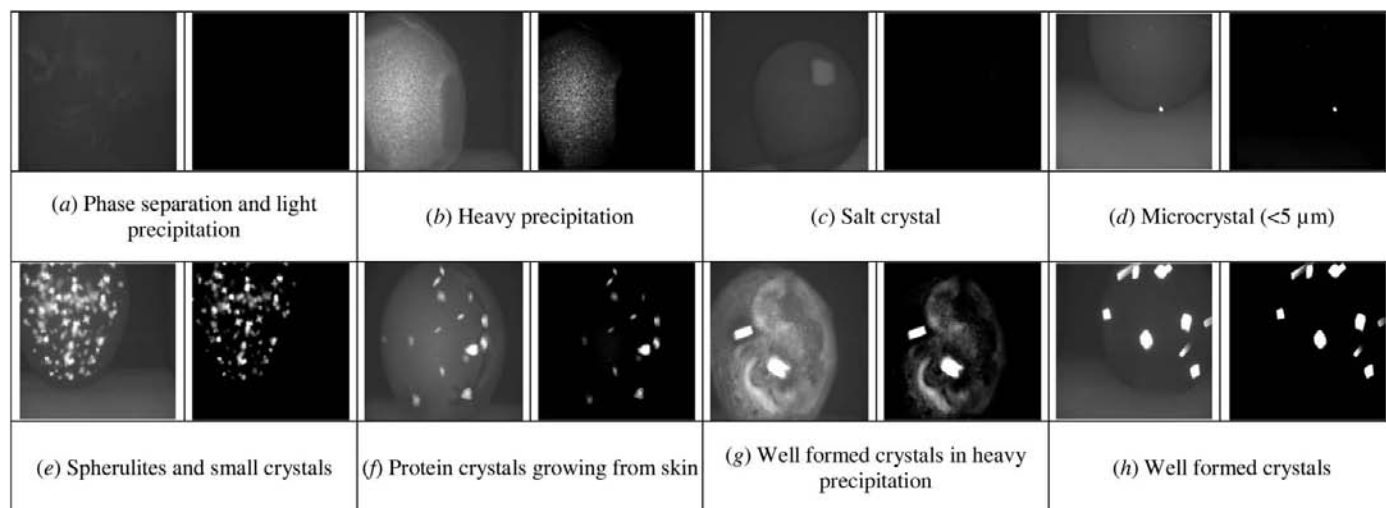

Figure 5
Image analysis of artifacts found within a typical crystallization experiment performed in the presence of 1,8-ANS. The images presented in Fig. 2 can be simply processed by the introduction of a threshold value. The images on the right of each pair show the effect when any pixel fluorescence intensity values <120 are set to zero. At this threshold, the signal from small protein microcrystals is still clearly visible (*d*), whereas the signal from phase separation (*a*) or salt crystals (*c*) has completely disappeared. Some signal is still obtained from crystallization conditions that contain heavy precipitate (*b* and *g*). However, manual visualization can clearly distinguish the presence of crystals in (*g*) from their absence in (*b*).

properties of a variety of different dyes that may display more advantageous properties in crystallization applications.

From our data, it is apparent that the addition of low concentrations of 1,8-ANS to crystallization experiments does not significantly adversely affect the production of protein crystals. The subsequent increase in fluorescence from the protein within these experiments is then available for analysis to determine the presence of protein crystals. While these images have all been examined manually for this report, it is not unreasonable to expect that the application of a simple intensity threshold to the crystallization images will result in the robust automated detection of even small protein micro-crystals.

References

Badger, J. (2003). *Acta Cryst.* D**59**, 823–827.

Berry, I. M., Dym, O., Esnouf, R. M., Harlos, K., Meged, R., Perrakis, A., Sussman, J. L., Walter, T. S., Wilson, J. & Messerschmidt, A. (2006). *Acta Cryst.* D**62**, 1137–1149.

Bourenkov, G. P. & Popov, A. N. (2006). *Acta Cryst.* D**62**, 58–64.

Forsythe, E., Achari, A. & Pusey, M. L. (2006). *Acta Cryst.* D**62**, 339–346.

Grundner, C., Ng, H. L. & Alber, T. (2005). *Structure*, **13**, 1625–1634.

Hartley, J. L. (2006). *Curr. Opin. Biotechnol.* **17**, 359–366.

Hiraki, M. *et al.* (2006). *Acta Cryst.* D**62**, 1058–1065.

Jancarik, J. & Kim, S.-H. (1991). *J. Appl. Cryst.* **24**, 409–411.

Judge, R. A., Swift, K. & González, C. (2005). *Acta Cryst.* D**61**, 60–66.

Kettenberger, H. & Cramer, P. (2006). *Acta Cryst.* D**62**, 146–150.

Kissinger, C. R., Gehlhaar, D. K. & Fogel, D. B. (1999). *Acta Cryst.* D**55**, 484–491.

Kouranov, A., Xie, L., de la Cruz, J., Chen, L., Westbrook, J., Bourne, P. E. & Berman, H. M. (2006). *Nucleic Acids Res.* **34**, D302–D305.

Lavault, B., Ravelli, R. B. G. & Cipriani, F. (2006). *Acta Cryst.* D**62**, 1348–1357.

Leslie, A. G. W. (1992). *Jnt CCP4/ESF–EAMCB Newsl. Protein Crystallogr.* **26**.

Leulliot, N., Quevillon-Cheruel, S., Sorel, I., de La Sierra-Gallay, I. L., Collinet, B., Graille, M., Blondeau, K., Bettache, N., Poupon, A., Janin, J. & van Tilbeurgh, H. (2004). *J. Biol. Chem.* **279**, 8351–8358.

McPherson, A. (1990). *Eur. J. Biochem.* **189**, 1–23.

Madhurantakam, C., Rajakumara, E., Mazumdar, P. A., Saha, B., Mitra, D., Wiker, H. G., Sankaranarayanan, R. & Das, A. K. (2005). *J. Bacteriol.* **187**, 2175–2181.

Mooij, W. T., Hartshorn, M. J., Tickle, I. J., Sharff, A. J., Verdonk, M. L. & Jhoti, H. (2006). *ChemMedChem*, **1**, 827–838.

Murshudov, G. N., Vagin, A. A. & Dodson, E. J. (1997). *Acta Cryst.* D**53**, 240–255.

Ness, S. R., de Graaff, R. A., Abrahams, J. P. & Pannu, N. S. (2004). *Structure*, **12**, 1753–1761.

Pan, S., Shavit, G., Penas-Centeno, M., Xu, D. H., Shapiro, L., Ladner, R., Riskin, E., Hol, W. & Meldrum, D. (2006). *Acta Cryst.* D**62**, 271–279.

Panjikar, S., Parthasarathy, V., Lamzin, V. S., Weiss, M. S. & Tucker, P. A. (2005). *Acta Cryst.* D**61**, 449–457.

Perrakis, A., Harkiolaki, M., Wilson, K. S. & Lamzin, V. S. (2001). *Acta Cryst.* D**57**, 1445–1450.

Perrakis, A., Sixma, T. K., Wilson, K. S. & Lamzin, V. S. (1997). *Acta Cryst.* D**53**, 448–455.

Pohl, E., Ristau, U., Gehrmann, T., Jahn, D., Robrahn, B., Malthan, D., Dobler, H. & Hermes, C. (2004). *J. Synchrotron Rad.* **11**, 372–377.

Popov, A. N. & Bourenkov, G. P. (2003). *Acta Cryst.* D**59**, 1145–1153.

Pothineni, S. B., Strutz, T. & Lamzin, V. S. (2006). *Acta Cryst.* D**62**, 1358–1368.

Rupp, B., Segelke, B. W., Krupka, H. I., Lekin, T., Schafer, J., Zemla, A., Toppani, D., Snell, G. & Earnest, T. (2002). *Acta Cryst.* D**58**, 1514–1518.

Slavik, J. (1982). *Biochim. Biophys. Acta*, **694**, 1–25.

Steen, J., Uhlen, M., Hober, S. & Ottosson, J. (2006). *Protein Expr. Purif.* **46**, 173–178.

Terwilliger, T. C. (2004). *J. Synchrotron Rad.* **11**, 49–52.

Terwilliger, T. C. & Berendzen, J. (1999). *Acta Cryst.* D**55**, 849–861.

Vernede, X., Lavault, B., Ohana, J., Nurizzo, D., Joly, J., Jacquamet, L., Felisaz, F., Cipriani, F. & Bourgeois, D. (2006). *Acta Cryst.* D**62**, 253–261.

Wilson, J. (2002). *Acta Cryst.* D**58**, 1907–1914.